Special Issue

Planar Iron Hydride Nanoclusters: Combined Spectroscopic and Theoretical Insights into Structures and Building Principles

Uttam Chakraborty,[a] Patrick Bügel,[b] Lorena Fritsch,[c] Florian Weigend,*[b, d] Matthias Bauer,*[c] and Axel Jacobi von Wangelin*[a]

In memory of Malcolm L. H. Green

The controlled assembly of well-defined planar nanoclusters from molecular precursors is synthetically challenging and often plagued by the predominant formation of 3D-structures and nanoparticles. Herein, we report planar iron hydride nanoclusters from reactions of main group element hydrides with iron(II) bis(hexamethyldisilazide). The structures and properties of isolated Fe_4, Fe_6, and Fe_7 nanoplatelets and calculated intermediates enable an unprecedented insight into the underlying building principle and growth mechanism of iron clusters, metal monolayers, and nanoparticles.

1. Introduction

Discrete planar metal nanoclusters are a rare class of materials between the regimes of monometallic coordination compounds and large metal particles.[1,2] While three-dimensional metal clusters can be viewed as structural models of the bulk material, small two-dimensional metal nanoclusters constitute intermediate stages of the growth of soluble metal complexes toward metallic monolayers (Figure 1).[1–9] Planar metal clusters exhibit unique geometries, magnetizations, and reactivities due to the stereoelectronic properties and intermetallic communication within the plane.[2b,3–9] Polynuclear metal carbonyls have been studied in great details but applications as materials and catalysts are rare.[1,2] The utilization of the smallest ligand, formal hydride ions, to support metal clusters has recently attracted great interest in the context of bond activations, reduction reactions, and hydrogen technologies.[3,9] Hydride-supported planar metal clusters M_xH_y ($x > 5$) are being targeted as competent molecular models of metal surfaces layered with hydrogen which are key intermediates of many hydrogen-based technologies including (de)hydrogenation reactions, the Haber-Bosch and Fischer-Tropsch processes, and fuel cells.[10] However, there are only a few metal hydride clusters reported in the literature, such as the homoleptic wheel-like Rh_7H_{18}.[7] Recently, Ohki *et al.* and our group have shown that simple substitutions

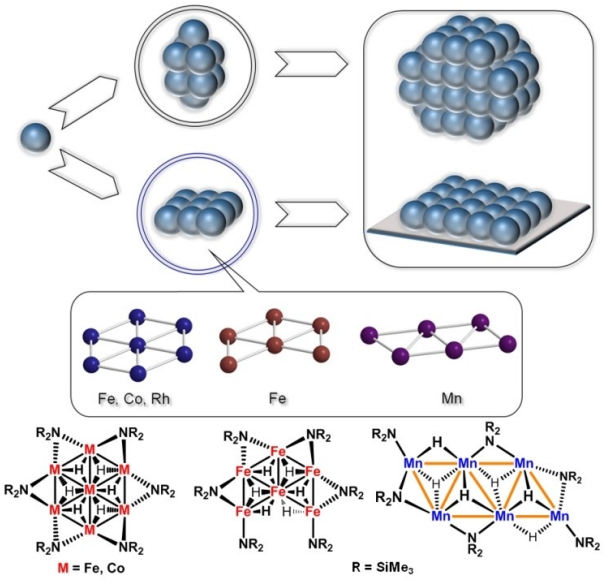

Figure 1. Discrete 2D and 3D transition metal clusters as molecular models of monolayers and bulk materials. Bottom: Recent examples of planar transition metal cluster topologies.

[a] *Dr. U. Chakraborty, Prof. Dr. A. Jacobi von Wangelin*
Dept. of Chemistry
University of Hamburg
Martin Luther King Pl. 6
20146 Hamburg (Germany)
E-mail: axel.jacobi@uni-hamburg.de
[b] *P. Bügel, Dr. F. Weigend*
Institut für Nanotechnologie
Karlsruher Institut für Technologie (KIT)
v.-Helmholtz Pl. 1
76344 Eggenstein-Leopoldshafen (Germany)
[c] *L. Fritsch, Prof. Dr. M. Bauer*
Dept. of Chemistry, Center for Sustainable Systems Design (CSSD)
University of Paderborn
Warburger Str. 100, 33098 Paderborn (Germany)
E-mail: bauerm@mail.uni-paderborn.de
[d] *Dr. F. Weigend*
Fachbereich Chemie
Philipps-Universität Marburg
Hans-Meerwein-Str. 4
35032 Marburg (Germany)
E-mail: florian.weigend@chemie.uni-marburg.de

Supporting information for this article is available on the WWW under https://doi.org/10.1002/open.202000307

Special Issue *An invited contribution to a Special Issue dedicated to Material Synthesis in Ionic Liquids.*

of bulky, low-valent metal(II) amides (M = Mn, Fe and Co) with main group element hydrides enabled the facile preparation of soluble planar $[M_xH_y(NR_2)_z]$ nanoclusters.[3–6] Examples include the $[Mn_6H_6(NR_2)_6]$ nanosheet,[3] the planar Co_4 cluster $[Co_4(NR_2)_4]$,[6] the Fe_4 trapeze $[(\eta^6\text{-toluene})Fe_4H_2(NR_2)_4]$, and the planar $Fe_{6,7}$ clusters $[Fe_6H_6(NR_2)_6]$ and $[Fe_7H_6(NR_2)_6]$ (Figure 1, bottom).[4,5] The Mn and Fe nanoclusters were demonstrated to represent instructive snapshots at the interface of homogeneous and heterogeneous hydrogenation catalysts as they served as soluble reservoirs of nanoparticle catalysts.[3,4]

The scarcity of planar metal cluster hydrides M_xH_y may be a direct consequence of the generally little insight into the growth mechanisms of small metal clusters and of the poor coordination properties of hydrides as bridging ligand in comparison to heteroatomic multi-dentate chelate ligands.[1a,b,d] A deeper understanding of the underlying building principles is essential to the rational design of new metal cluster topologies and materials properties. Despite the isolation of homologous metal hydride clusters of the formula $[M_xH_y(NR_2)_z]$ (M = Mn, Fe, Co; R = $SiMe_3$), the mechanistic details of their formation from the molecular precursors $[M(NR_2)_2]$ have remained unknown.[3] The availability of new Fe_4H_2, Fe_6H_6, and Fe_7H_6 clusters prompted experimental and theoretical studies into the structures, properties, and cluster growth mechanisms of this concise family of Fe clusters which may have direct ramifications for the control of 2D cluster topologies and the access to metal monolayers.

2. Synthesis and Characterization of μ²-Amido Ironhydride Clusters

The formation of metal hydride clusters from stoichiometric reactions of the low-valent $Fe(hmds)_2$ (hmds = hexamethyldisilazide, $N(SiMe_3)_2$) with diisobutylaluminium hydride (Dibal–H) was highly sensitive to the employed solvent.[4] Reactions in toluene and hexane afforded the tetranuclear iron hydride cluster $[(\eta^6\text{-toluene})Fe_4H_2(hmds)_4]$ (**1**) in 38% yield (Figure 2A). The unusual planar Fe_4 core contained two different sets of iron centers, bridging amido and hydrido ligands. The identical complex was isolated by Ohki et al. from the related reaction with pinacolborane in toluene.[5] As the cluster topology was highly dependent on the stoichiometry of $Fe(hmds)_2$ and hydride reagent, we performed a reaction involving sequential addition of $Fe(hmds)_2$ and Dibal–H (1 : 2) followed by another equiv. of $Fe(hmds)_2$ in toluene. The resulting crude product was analyzed by LIFDI-MS (Figure 2B). The major peak at m/z = 864.17 indicated clean formation of a different Fe_4 cluster with the composition $[Fe\{N(SiMe_3)_2\}]_4$. However, elimination of H atoms during MS analysis cannot be excluded. We postulate that the resultant tetranuclear amidoiron cluster adopts a similar square-planar topology as the homologous Co_4 cluster from the reduction of $Co\{N(SiMe_3)_2\}_2$ with pinBH.[6] Further characterizations of the elusive $[Fe\{N(SiMe_3)_2\}]_4$ complex could not be obtained due to rapid degradation under the

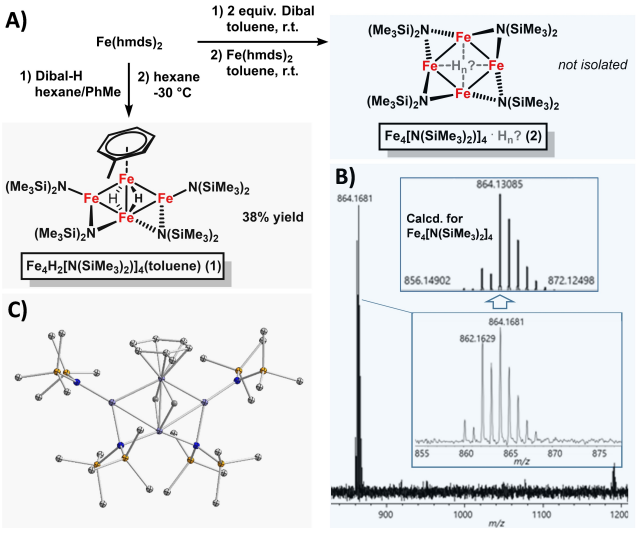

Figure 2. Fe_4 clusters. A) Preparation from iron(II) bis(hexamethyldisilazide); B) experimental (LIFDI-MS, THF) and calculated mass spectra (upper inset).

reaction conditions. Related tetra-nuclear clusters were reported for Ni[11] and coinage metals.[12]

The isolated cluster $[(\eta^6\text{-toluene})Fe_4H_2(hmds)_4]$ (**1**) was characterized by crystal structure analysis (Figure 2C), NMR spectroscopy, and elemental analysis. **1** contains a rare planar Fe_4 core that is peripherally bridged by two μ_2-$N(SiMe_3)_2$ ligands; two amides are terminally bound.[4,5] One Fe is coordinated by the solvent toluene in η^6-mode. The Fe–Fe distances in **1** range from 2.4740(5) to 2.6425(4) Å, with the internal Fe–Fe bond bearing the μ^2-hydrides being shortest. The presence of the hydride ligands was determined by crystal structure analysis and IR spectroscopy[5] and also with x-ray emission spectroscopy (*vide infra*). The ^{1}H-NMR spectrum of the paramagnetic compound in C_6D_6 showed broad signals at δ = −22.7, −20.6, −12.1 and 52.8 ppm for the coordinated toluene; the amides gave two sets of broad singlet resonances at δ = −5.31 and −1.83 ppm. **1** exhibited a melting point of 123 °C. The Mössbauer spectrum of **1** is in perfect agreement with a formal $[Fe^0{}_1Fe^{II}{}_3]$ complex as reported by Ohki et al..[5]

Reaction of $Fe[N(SiMe_3)_2]_2$ with equimolar Dibal–H in *n*-hexane and crystallization at −30 °C afforded a mixture of two larger nanoclusters, the hexairon compound $[Fe_5(hmds)_6FeH_6]$ (**3**) and $[Fe_6(hmds)_6FeH_6]$ (**4**), in 35% overall yield as a 4 : 1 mixture (Figure 3A). The clusters co-crystallized and showed compositional disorder. Gratifyingly, we obtained a pentagonal single crystal of **3** from the reaction of $Fe[N(SiMe_3)_2]_2$ and Dibal–H (1 : 1) in *n*-hexane. All six H ligands were located in the Fourier differential map with similar bond parameters as the reported Fe_6/Fe_7 co-crystallized structures. Further support of the presence of hydride ligands was derived from LIFDI-MS spectra of the **3** + **4** cluster mixture in toluene (Figure 3C). The hexa-iron cluster **3** exhibited a peak at m/z = 1300.18 with an isotope pattern of [**3**]-2H where dihydrogen was eliminated from the parent compound (calcd. m/z = 1301.23). The hepta-iron cluster **4** gave the molecular ion [**4**] as the major peak at m/z = 1358.14 (calcd. m/z = 1358.18). The clusters were further

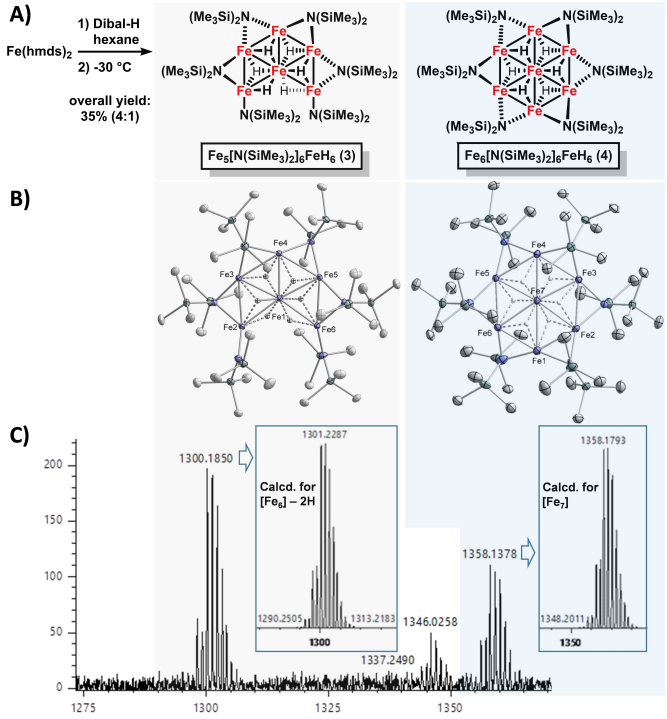

Figure 3. Fe_6/Fe_7 clusters. A) Preparation from $Fe(hmds)_2$; B) crystal structures; C) experimental (LIFDI-MS, toluene-d_8) and calculated mass spectra (insets).

characterized by elemental analysis and NMR. The ^{1}H NMR of the paramagnetic mixture **3** + **4** in C_6D_6 displayed broad signals at $\delta = -16.3$, -3.3 and at -29.7 ppm.

2.1. Hard X-Ray Spectroscopy

The electronic structure of the Fe_4 cluster **1** was studied by hard X-ray spectroscopy. High-energy resolution fluorescence-detected X-ray absorption near-edge spectroscopy (HERFD-XANES)[13] and X-ray emission spectroscopy (XES)[14–16] provide valuable insight into the local electronic structure of 3d-metal complexes. XANES spectra of 3d-metal complexes exhibit in their pre-edge region 1 s→nd transitions to unoccupied states so that LUMO states can be probed.[17] However, detailed information on LUMO states are often limited by the experimental resolution due to the 1 s core-hole lifetime broadening in the final state. The experimental resolution can be enhanced if a long-lived emissive final state is detected, as the minimal signal linewidth is inversely proportional to the lifetime of the associated final state (HERFD-XANES).[18,19] Additionally, K-edge valence-to-core X-ray emission spectroscopy (VtC XES)[20] is a powerful tool to analyze the emission caused by electron relaxation into the 1 s-orbital after electronic excitation at energies above the absorption edge. Thus, VtC-XES serves as a probe of valence levels including occupied 3d-orbitals and ligand-centered orbitals.[21] Since a 3d→1 s transition is dipole-forbidden, 4p-mixing would increase the transition intensity. Therefore, K-edge VtC-XES and pre-edge XANES spectroscopy specifically determine where hybridization in the donor orbital effects significant metal 4p-character. The high symmetry of octahedral complexes[22] results in weak 3d-features; tetrahedral complexes give intense 3d-bands.[23] A similar effect is observed for transitions from ligand orbitals to the metal 1 s-orbital which are only observed at significant overlap between ligand and metal 4p orbitals.[23] Lastly, hard X-ray spectroscopy may also provide insight into spin multiplicities of metal complexes. As a first approximation from hard X-ray HERFD-XANES and VtC-XES, we calculated the crystal structure[5] single-point energies of **1** at different electron spin multiplicities with the TPSS functional and def2-TZVPP basis set (broken symmetry calculations were not considered). A mixed-valence $[(Fe^{II})_3(Fe^0)_1]$ core may display a maximum spin multiplicity M_S of 15. A singlet configuration was excluded due to the paramagnetism of **1**[4,5] and the calculated single point energies (Figure 4A). The experimental HERFD-XANES and VtC spectra were compared with theoretical data to analyze the probable spin states of **1**. XANES spectra showed very good agreement between experiment and theory with M_S 3, 9, 11, and 15. (Figure 4B). Two distinct absorptions were observed at 7112.5 eV and 7117 eV: Signal *1* is the 1 s→3d transition; signal *2* could result from transitions into mixed orbitals of 45% Fe(p + d) and 18–31% H(s,p) (see Table S1, Figure S7). The simulated XANES spectra of M_S 5, 7 and 13 states showed poor spectral agreement, mostly due to the absence of the characteristic 1 s→3d transition at 7112.5 eV. The experiment also lacked the weak 7114.5 eV band of all calculated spectra which may be due to overestimated transitions into mixed orbitals of 50% Fe(s + p + d) and 11% C(s + p) character (see Table S1). Further insight into the electronic structure of **1** was gained from VtC-XES spectra. Figure 4C documents that all calculated spectra are very similar in shape and intensity. The Kβ″ signal at 7095 eV derives from transitions from C(s) (7092 eV) and N(s) (7095.5 eV) orbitals; the $K\beta_{2,5}$ signal results from transitions from molecular orbitals of 44% C(p) and 14% H(s) (at 7105 eV) character and from Fe(d) orbitals (at 7110 eV). A slight variation of signal intensities is observed as the Fe d-orbitals are directly influenced by the spin multiplicity. Interestingly, the calculated $M_s = 15$ spectrum showed an additional high-energy signal at 7114 eV which matches that of the experiment and presumably originates from Fe(d)→1 s transitions of the μ-H–Fe ions (see Table S2). The bridging hydrides in complex **1** were observed by crystal structure analysis and IR spectroscopy.[4,5] The VtC signal is especially sensitive towards metal–hydride interactions.[23,24] Direct comparison of the experimental VtC spectrum of **1** and theoretical spectra derived from DFT calculations proved the presence of iron hydride motifs (Figure 4D). The major signal at 7107 eV and the shoulder at 7110 eV showed high reproducibility only with a μ^2-dihydrido Fe_4 structure. An MO analysis of the calculated transitions revealed that an intense transition into a mixed orbital of C(p) and H(s) orbitals (9% hydridic) is observed at 7105.1 eV (see Table S2). These results are in full agreement with earlier studies of the tetrahydride complex $[\{CpFe\}_2(\mu\text{-}H)_4]$ which involved a similar 7107 eV emission of the H–Fe motifs.[24]

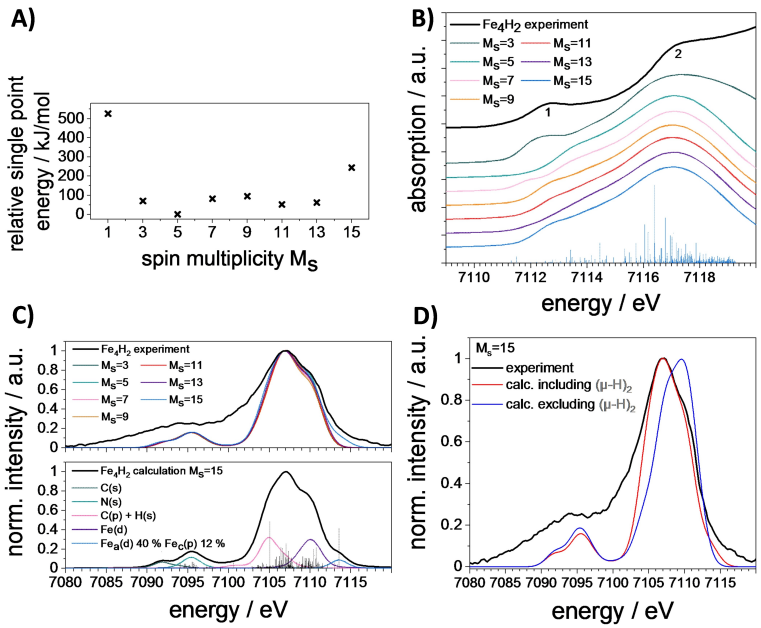

Figure 4. A) Relative single-point energies of different spin multiplicities of **1**. B) Top: Experimental (grey) and theoretical (colored) HERFD-XANES spectra of **1** in different spin multiplicities. Bottom: Energies of electronic transitions of $M_s = 15$ without line-broadening. C) Experimental VtC-XES and calculated spectra of different multiplicities (top). Deconvolution of orbital contributions to the VtC spectrum calculated for cluster **1** with $M_s = 15$ (bottom). D) Experimental and theoretical VtC spectra of **1** with and without μ_2-hydrides ($M_s = 15$).

2.2. Cluster Growth Mechanism

The mechanism of amidoiron hydride cluster formation is presumably initiated with a formal σ-bond metathesis between a Fe–NR_2 bond and the main group element hydride E–H (E = R'_2Al or R'_2B) and is driven by the high bond energy in E–NR_2. The resultant coordinatively highly unsaturated [Fe(hmds)H] can thus be viewed as the monomeric repeating unit of subsequent cluster growth. The formation of a dimer, most likely involving μ^2-H-bonding motifs, is in full accord with the observation of similar [$(hmds)_2(\mu\text{-}X)_2Fe_2$] species with the bulky hmds ligand.[25] The formal [1 + 2]-addition of [Fe(hmds)H] onto such dimer would result in the generation of a non-linear but planar M_3 unit which appeared to be the common motif of all members of the $(hmds)_xM_yH_z$ family with Mn_6, Fe_4, Fe_6, Fe_7, and Co_7 cores. In an effort to gain further insight into the mechanistic details of such cluster growth, we performed DFT calculations on each [$M_1 + M_n$] addition step from the mono-metallic precursors to the largest isolated cluster of this series (see the Supporting Information for details). We postulate a stepwise addition of the formal repeating unit [Fe(hmds)H] in the individual reactions R2 to R7 (Figure 5, top). R1, the formation of [Fe(hmds)H] from $Fe(hmds)_2$, is exothermic by 366 kJ mol^{-1}. This number is diminished by the energy needed for the formation of two H atoms, which is in the same range, if a typical covalent bond needs to be broken. The reactions R2 to R6 are all highly exothermic (R2 = −208, R3 = −235, R4 = −181, R5 = −285, R6 = −241, all in kJ mol^{-1}). The final addition of the mono-metallic entity Fe(hmds)H to M6, reaction R7, involves elimination of hexamethyldisilazane (hmds–H). R7 was determined to be even more exothermic (−302 kJ mol^{-1}). Consequently, thermodynamic arguments are in full support of the formation of the Fe_7 cluster **4** via the proposed pathway. Kinetic considerations are also not prohibitive of such mechanism. Exemplarily, the energy profile for the formal [$M_2 + M$] addition according to R2 was calculated (Figure 5, bottom). A very low barrier of 13 kJ mol^{-1} was calculated when the hydride ligand of M approaches the TMS substituents of M_2, which easily can be overcome at room temperature. The mechanistic trajectory of the underlying Fe_3-triangle formation is further illustrated by a movie in the Supporting Information. We finally investigated the stability of M_2 and M_4 toward the abstraction of two H atoms, *i.e.* dehydrogenation (Figure 5, inset). H_2 elimination from M_2 is thermodynamically disfavored by 173 kJ mol^{-1}. In contrast, the corresponding reaction energy for M_4 is negative (−41 kJ mol^{-1}). Further, the remaining two H atoms are only weakly bound (22 kJ mol^{-1}), so that M_4 is expected to be an unstable intermediate en route to the larger Fe_n clusters.

3. Conclusions

The rapid aggregation of coordinatively unsaturated metal complexes to larger metal particles under reducing conditions makes the isolation and characterization of intermediate cluster sizes especially challenging. Very little is known about the coordination chemistry, topology, and growth mechanism of discrete metal nanoclusters. Upon reaction of simple iron(II) bis (hexamethyldisilazide) with hydroborane/alane derivatives, various planar iron nanoclusters could be isolated and studied by theoretical and experimental techniques. For the first time, hard X-ray spectroscopy (HERFD-XANES, VtC-XES) was applied to

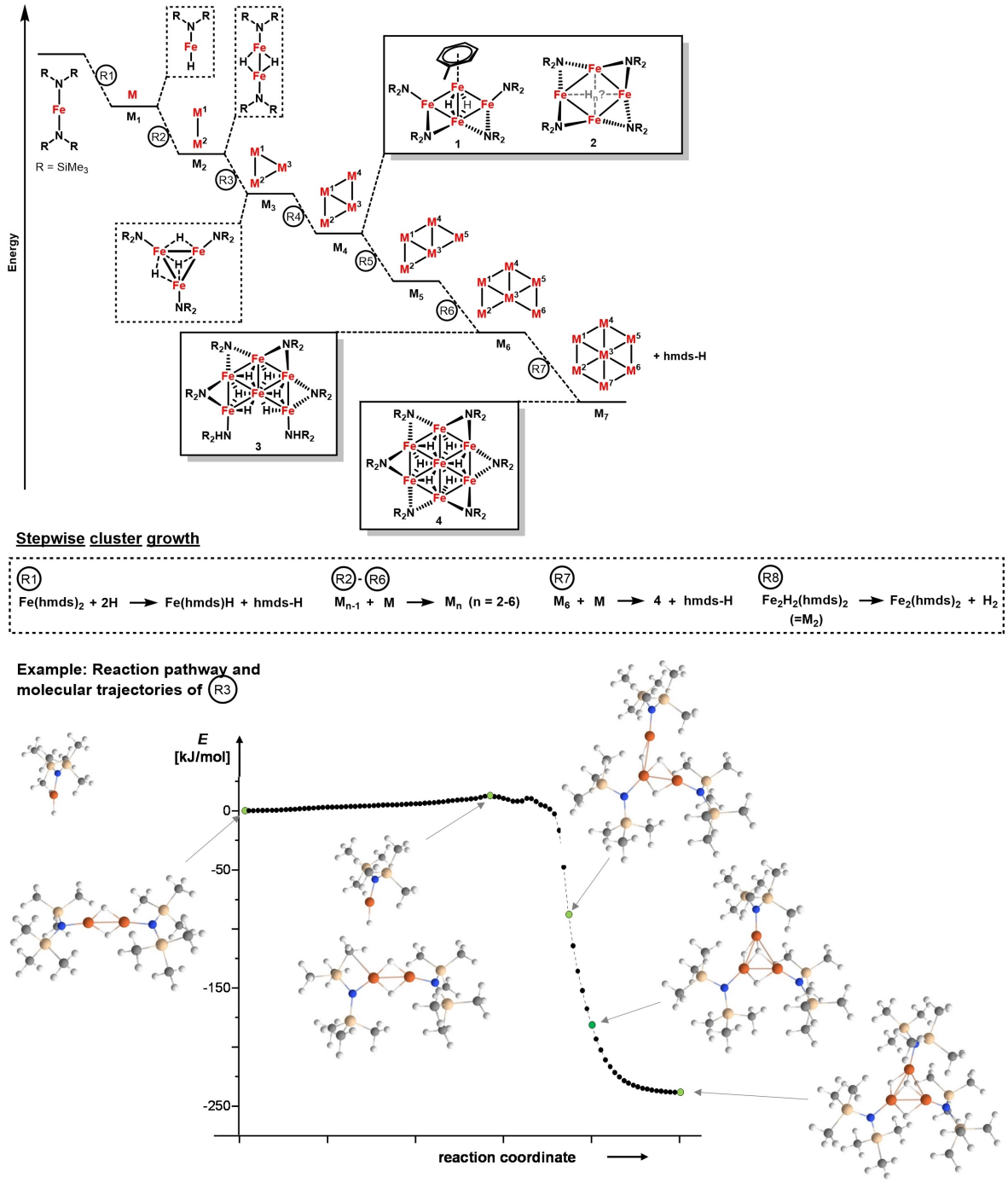

Figure 5. Top: Proposed mechanism of the formation of $[Fe(hmds)H]_n$ clusters. Solid boxes: isolated clusters; dashed boxes: calculated structures. hmds = $N(SiMe_3)_2$, hmds–H = $N(SiMe_3)_2H$, M=Fe(hmds)H. Bottom: Energy profile of the reaction pathway R3 from M_2 + M to M_3. The depicted intermediate structures refer to the points plotted in green. Fe atoms are shown in brown, N in blue, Si in beige, C in grey, and H in light grey.

such cluster complexes to complement magnetic measurements (Evans, SQUID) that postulated high spin multiplicities. Further, VtC-XES supported the presence of iron hydride moieties. The unusual formation of planar iron clusters was further analyzed by DFT calculations which gave strong support of a stepwise mechanism involving the key role of hydridoiron amide additions to Fe–Fe oligomers. The isolation of intermediate cluster sizes (n = 4–7) is most likely a direct consequence of kinetic aggregation barriers from the bulky amido ligands and the low concentration of reactive hydridoiron monomers whereas the growth to larger clusters is thermodynamically highly favored. The application of hard X-ray spectroscopy and DFT to such large and stereoelectronically unusual metal clusters is not trivial and with very little precedents, but both methods have been demonstrated to provide new insight into structure and reactivity of such complex systems. This study has

significantly deepened the understanding of planar metal cluster growth mechanisms which may have direct ramifications for the assembly of metal monolayer materials.

Experimental Section

HERFD-XANES and VtC-XES were performed at beamline ID26 of the European Synchrotron Radiation Facility ESRF (Grenoble, France). The solid samples were prepared as wafers using BN as a binder. All measurements were carried out at 50 K with a He cryostat under vacuum conditions. The incident energy was selected by a Si double crystal mono-chromator using the ⟨311⟩ reflection. Ge⟨620⟩ crystal analyzers were used for detection in a Johann-type X-ray emission spectrometer under He atmosphere to reduce the absorption of fluorescence radiation. HERFD-XANES spectra at the Fe K-edge were obtained by recording the Fe Kβ1,3 emission line as a function of the incident energy. For the VtC-XES data collection, an incident energy of 7200 eV was chosen; the energy scans were carried out between 7065 and 7140 eV. No radiation damage was observed within the acquisition time, and measurements were carried out on multiple spots. The VtC-XES spectra are super-imposed by the high-energy slope of the Kβ1,3 emission line and were background-corrected: The slope was fitted and the experiments subtracted by the resulting fit. Normalization of VtC-XES and HERFD-XANES spectra was achieved by dividing each point by the sum of all intensity values. Computations for XAS/XES interpretations were performed with ORCA 4.2.1.[26] Theoretical VtC-XES (DFT)[21] and XANES (TD-DFT)[26a,b] spectra were calculated using the TPSS functional[27] and the def2-TZVPP basis set,[28] combined with the def2/J auxiliary basis set.[29] DFT grid 7 was used for Fe. Dispersion correction was included, Becke-Johnson damping scheme (D3BJ).[30,31] For further analysis, MOAnalyzer was used.[32] The calculated spectra were shifted to match the 7117 eV peak (XANES) or the Kβ2,5 peak at 7107 eV (VtC-XES), by 170 eV (XANES) and 170.6 eV (VtC-XES), respectively, and normalized to these maxima. XANES (TD-DFT) transitions were broadened with Gaussian fwhm starting at 0.6 eV for the prepeak, and linearly rising with increasing excitation energy. The VtC-XES spectra are broadened with a fixed fwhm of 3 eV. The Kohn-Sham orbitals were visualized with IboView (vers. 20150427).[33,34] Orbital populations were extracted via Löwdin reduced orbital population analysis. For further details, see the Supporting Information.

DFT calculations of the cluster growth were done with TURBOMOLE[35] employing the TPSS functional[36] and def2-SVP basis sets.[37] Integration grids were of fine size (grid 5), for all further input parameters default values were applied. All presented structures of the cluster growth study are minimum structures (Figure 5), as checked by the calculation of vibration frequencies. For all complexes, high-spin states were calculated. Total energies, numbers of unpaired electrons, and Fe–Fe distances are listed in the Supporting Information. Reaction pathway R3 was calculated with the method proposed by Plessow[38] with 93 intermediates between initial and final state; here medium size grids (grid 3) were chosen for economy. The initial state, M_2+M, was obtained from the final state M_3 by moving one of the M units 20 Bohr along a vector defined by one of the Fe–Fe edges in M_3 and optimizing the entire system with fixed distance between M_2 and M. Cartesian coordinates for Fe complexes are available in the Supporting Information.

Acknowledgements

This work was supported by Deutsche Forschungsgemeinschaft (SPP 1708) and the European Research Council (CoG 683150).

Conflict of Interest

The authors declare no conflict of interest.

Keywords: density functional calculations · iron · metal clusters · metal hydrides · X-ray spectroscopy

[1] Reviews: a) C. E. Holloway, M. Melnik, *J. Organomet. Chem.* **1990**, *396*, 129; b) P. Braunstein, L. A. Oro, P. R. Raithby, *Metal Clusters in Chemistry*, Wiley-VCH, Weinheim, **1999**; c) L. Guczi, A. Beck, A. Horváth, D. Horváth, *Top. Catal.* **2002**, *19*, 157; d) D. M. P. Mingos, R. H. Crabtree, *Comprehensive Organometallic Chemistry III*, Elsevier, Amsterdam, **2007**, 1st ed., Vols. 5–6; e) S. Zacchini, *Eur. J. Inorg. Chem.* **2011**, *2011*, 4125; f) P. Buchwalter, J. Rosé, P. Braunstein, *Chem. Rev.* **2015**, *115*, 28; g) I. Chakraborty, T. Pradeep, *Chem. Rev.* **2017**, *117*, 8208.
[2] a) P. Buchwalter, J. Rosé, P. Braunstein, *Chem. Rev.* **2015**, *115*, 28; b) M. T. Nielsen, R. Padilla, M. Nielsen, *J. Cluster Sci.* **2020**, *31*, 11.
[3] U. Chakraborty, E. Reyes-Rodriguez, S. Demeshko, F. Meyer, A. Jacobi von Wangelin, *Angew. Chem. Int. Ed.* **2018**, *57*, 4970.
[4] T. N. Gieshoff, U. Chakraborty, M. Villa, A. Jacobi von Wangelin, *Angew. Chem. Int. Ed.* **2017**, *56*, 3585.
[5] R. Araake, K. Sakadani, M. Tada, Y. Sakai, Y. Ohki, *J. Am. Chem. Soc.* **2017**, *139*, 5596.
[6] Y. Ohki, Y. Shimizu, R. Araake, M. Tada, W. M. C. Sameera, J.-I. Ito, H. Nishiyama, *Angew. Chem. Int. Ed.* **2016**, *55*, 15821.
[7] S. K. Brayshaw, J. C. Green, R. Edge, E. J. L. McInnes, P. R. Raithby, J. E. Warren, A. S. Weller, *Angew. Chem. Int. Ed.* **2007**, *46*, 7844.
[8] E. Cerrada, M. Contel, A. D. Valencia, M. Laguna, T. Gelbrich, M. B. Hursthouse, *Angew. Chem. Int. Ed.* **2000**, *39*, 2353.
[9] 2D metal clusters with CO ligands: a) R. D. Adams, Q. Zhang, X. Yang, *J. Am. Chem. Soc.* **2011**, *133*, 15950 and references therein; b) S. Du, B. E. Hodson, P. Lei, T. D. McGrath, F. G. A. Stone, *Inorg. Chem.* **2007**, *46*, 6613; c) G. Kong, G. N. Harakas, B. R. Whittlesey, *J. Am. Chem. Soc.* **1995**, *117*, 3502; d) M. P. Diebold, S. R. Drake, B. F. G. Johnson, J. Lewis, M. McPartlin, H. Powell, *J. Chem. Soc. Chem. Commun.* **1988**, 1358; e) G. Doyle, K. A. Eriksen, D. van Engen, *J. Am. Chem. Soc.* **1986**, *108*, 445.
[10] *Hydrogen in Metals III. Properties and Applications.* (Ed.: H. Wipf), Springer, Berlin, **1997**.
[11] M. Faust, A. M. Bryan, A. Mansikkamäki, P. Vasko, M. M. Olmstead, H. M. Tuononen, F. Grandjean, G. J. Long, P. P. Power, *Angew. Chem. Int. Ed.* **2015**, *54*, 12914.
[12] S. D. Bunge, O. Just, W. S. Rees, Jr., *Angew. Chem. Int. Ed.* **2000**, *39*, 3082 and references therein.
[13] A. J. Atkins, M. Bauer, C. R. Jacob, *Phys. Chem. Chem. Phys.* **2013**, *15*, 8095.
[14] P. Glatzel, U. Bergmann, *Coord. Chem. Rev.* **2005**, *249*, 65.
[15] U. Bergmann, P. Glatzel, *Photosynth. Res.* **2009**, *102*, 255.
[16] M. Bauer, *Phys. Chem. Chem. Phys.* **2014**, *16*, 13827.
[17] A. J. Atkins, C. R. Jacob, M. Bauer, *Chem. Eur. J.* **2012**, *18*, 7021.
[18] K. Hämäläinen, D. P. Siddons, J. B. Hastings, L. E. Berman, *Phys. Rev. Lett.* **1991**, *67*, 2850.
[19] F. M. F. De Groot, M. H. Krisch, J. Vogel, *Phys. Rev. B - Condens. Matter Mater. Phys.* **2002**, *66*, 1.
[20] M. U. Delgado-Jaime, S. Debeer, M. Bauer, *Chem. Eur. J.* **2013**, *19*, 15888.
[21] N. Lee, T. Petrenko, U. Bergmann, F. Neese, S. DeBeer, *J. Am. Chem. Soc.* **2010**, *128*, 9715.
[22] F. Neese, *Inorg. Chim. Acta* **2002**, *337*, 181.
[23] L. Burkhardt, M. Holzwarth, B. Plietker, M. Bauer, *Inorg. Chem.* **2017**, *56*, 13300.
[24] L. Burkhardt, C. Mueller, O. A. Groß, Y. Sun, H. Sitzmann, M. Bauer, *Inorg. Chem.* **2019**, *58*, 6609.

[25] a) M. M. Olmstead, P. P. Power, S. C. Shoner, *Inorg. Chem.* **1991**, *30*, 2547; b) S. Yogendra, T. Weyhermüller, A. W. Hahn, S. DeBeer, *Inorg. Chem.* **2019**, *58*, 9358.
[26] a) S. DeBeer, George, T. Petrenko, F. Neese, *Inorg. Chim. Acta* **2007**, *361*, 965; b) S. DeBeer, George, F. Neese, *Inorg. Chem.* **2010**, 49, 1849; c) F. Neese, F. Wennmohs, U. Becker, C. Riplinger, *J. Chem. Phys.* **2020**, *152*, 224108.
[27] V. N. Staroverov, G. E. Scuseria, J. Tao, J. P. Perdew, *J. Chem. Phys.* **2003**, *119*, 12129.
[28] F. Weigend, R. Ahlrichs, *Phys. Chem. Chem. Phys.* **2005**, *7*, 3297.
[29] F. Weigend, *Phys. Chem. Chem. Phys.* **2006**, *8*, 1057.
[30] S. Grimme, J. Antony, S. Ehrlich, H. Krieg, *J. Chem. Phys.* **2010**, *132*, 154104.
[31] S. Grimme, S. Ehrlich, L. Goerigk, *J. Comput. Chem.* **2011**, *32*, 1456.
[32] M. U. Delgado-Jaime, S. DeBeer, *J. Comput. Chem.* **2012**, *33*, 2180.
[33] G. Knizia, *J. Chem. Theory Comput.* **2013**, *9*, 4834.
[34] G. Knizia, J. E. M. N. Klein, *Angew. Chem. Int. Ed.* **2015**, *54*, 5518.
[35] TURBOMOLE V7.5 **2020**, Turbomole GmbH; available from http://www.turbomole.com.
[36] J. Tao, J. P. Perdew, V. N. Staroverov, G. E. Scuseria, *Phys. Rev. Lett.* **2003**, *91*, 146401.
[37] F. Weigend, R. Ahlrichs, *Phys. Chem. Chem. Phys.* **2005**, *7*, 3297.
[38] P. Plessow, *J. Chem. Theory Comput.* **2013**, *9*, 1305.

Manuscript received: October 10, 2020
Revised manuscript received: February 17, 2021